MRI Reconstruction using Real-Time Motion Tracking: A Simulation Study

Jeff Orchard
David R. Cheriton School of Computer Science
University of Waterloo
Waterloo, ON Canada, N2L 3G1
e-mail: jorchard@uwaterloo.ca

Robert Staruch
Department of Medical Biophysics
University of Toronto
Toronto, ON Canada, M5G 2M9
e-mail: staruchr@sri.utoronto.ca

***Abstract*—Previous efforts to compensate for patient motion in MRI invariably assume that the patient is motionless for some part of the scan. In this paper, we propose the use of motion-tracking data to enable motion-correction during the entire scan, including the acquisition stage. Using a simulated MRI scanner, we compare the different ways to use the motion-tracking data (both retrospectively and prospectively) and compare the reconstruction results to motion compensation using navigator echoes. The results show that full motion compensation can reduce motion artifacts that navigator methods miss.**

***Index Terms*—MRI, motion correction, reconstruction, motion-tracking.**

I. Introduction

Patient motion is one of the most critical issues in modern-day magnetic resonance imaging (MRI). If a patient moves during a five-minute scan, the collected images could contain errors that render the images useless, wasting the time of the radiologist, and the MR suite (not to mention the lost time in the race to diagnose a disease). Motion-correction for MRI is an active field of research. Here, we focus on rigid-body motion only.

In some MRI scan sequences, the intra-echo pause can last as long as 200 ms. A patient with tremors could easily move during this 200 ms window, making MR imaging methods such as diffusion imaging and flow imaging nearly impossible. Unfortunately, the patients who need these imaging protocols often have difficulty staying still. None of the motion-correction techniques developed to date can address this issue. Correcting this kind of motion would make it possible to acquire important motion-sensitive images for the diagnosis and analysis of ailments such as multiple sclerosis, strokes, arteriovenous malformations, and other cerebrovascular diseases.

An MRI scan sequence is composed of many (approx. 100 to 200) excitation-acquisition repetitions. Many MRI motion-correction techniques aim only to measure and correct the motion increment that occurs between phase encodes (a "phase encode" is one line of samples in k-space). Some of these methods try to derive the patient motion by minimizing the entropy of the reconstructed image (known as autofocussing) [1], while some other methods use standard registration techniques on high-speed, low-resolution images called navigator echoes (NAVs) acquired between phase encodes [2]. Finally, a few groups have started to monitor and correct patient motion using motion-tracking systems [3], [4].

Despite the fact that some work has been done to develop the theory of full motion-correction [5], [6], [7], [8], no one to our knowledge has suggested the use of this motion-tracking data to correct for motion that occurs *at all points* during the scan.

The premise of this project is to use motion-tracking data in the reconstruction process to undo the effects of patient motion at all stages of the scanning process. The concept is to acquire patient motion throughout the MR scan using an optical motion-tracking camera system. This motion data can be used either in a post-processing environment to compute a much better estimate to the tissues phase state, or prospectively to update the scanning parameters [4], [9], [10].

II. Theory

A. MR Signal

The signal measured in MRI is a function of time,

$$S(t) = \int f(\vec{x})\, e^{-j\gamma \int^t \vec{G}(\tau)\cdot\vec{x}\, d\tau}\, d\vec{x}, \tag{1}$$

where $\vec{x}$ represents a position inside the scanner bore, $f(\vec{x})$ is the (transverse magnetization) function being imaged, $\vec{G}(\tau)$ is a vector that describes the magnetic field gradients, and γ is the gyromagnetic ratio [11]. The signal is a function of time because we can only sample a single Fourier coefficient at a time. To see this, notice that if

$$\vec{k}(t) = \gamma \int^t \vec{G}(\tau)\, d\tau, \tag{2}$$

then the MRI signal is simply the Fourier transform (FT) of the function f. To collect an entire image, we vary the external magnetic field gradients ($\vec{G}(t)$) over time to traverse the spatial frequency domain (k-space).

B. Motion Corruption

If the patient moves, then we replace f in (1) with a time-varying function $\overline{f}$, and (1) becomes

$$S(t) = \int \overline{f}(\vec{x}, t) e^{-j\gamma \int^t \vec{G}(\tau)\cdot\vec{x}\, d\tau}\, d\vec{x} \tag{3}$$

where the integral over $\vec{x}$ is taken with respect to a reference frame fixed to the MR scanner. If the integral traversed the volume with respect to an anatomy-fixed reference frame, then the corresponding f would not depend on time. Hence, we define the change of variables

$$\begin{aligned} \vec{u} &= \mathbf{R}(t)\vec{x} + \vec{T}(t) \\ \Rightarrow \vec{x} &= \mathbf{R}^{-1}(t)\left(\vec{u} - \vec{T}(t)\right), \end{aligned}$$

where $\mathbf{R}(t)$ is a time-varying rotation matrix, and $\vec{T}(t)$ is a time-varying translation vector. Assuming that $\mathbf{R}$ and $\vec{T}$ are chosen to match the motion of the patient, (3) can be written

$$S(t) = \int f(\vec{u}) e^{-j\gamma \int^t \vec{G}(\tau)\cdot \mathbf{R}^{-1}(\tau)\left(\vec{u}-\vec{T}(\tau)\right)d\tau} d\vec{u} \quad (4)$$

$$= \int f(\vec{u}) e^{-j\gamma \int^t \mathbf{R}(\tau)\vec{G}(\tau)\cdot\left(\vec{u}-\vec{T}(\tau)\right)d\tau} d\vec{u}. \quad (5)$$

In this anatomy-fixed context, the essence of the patient's rotation is incorporated by an equivalent rotation of the magnetic field gradients. The phase integral,

$$\phi(t) = \gamma \int^t \mathbf{R}(\tau)\vec{G}(\tau) \cdot \left(\vec{u} - \vec{T}(\tau)\right) d\tau, \quad (6)$$

can be broken into two terms: one that depends on $\vec{u}$, and one that does not,

$$\begin{aligned} \phi(t) &= \gamma \int^t \mathbf{R}(\tau)\vec{G}(\tau)\cdot\vec{u}d\tau - \gamma\int^t \mathbf{R}(\tau)\vec{G}(\tau)\cdot\vec{T}(\tau)d\tau \\ &= \vec{\phi}_{\mathbf{R}}(t)\cdot\vec{u} - \phi_{\vec{T}}(t)\,. \end{aligned} \quad (7)$$

The MR signal is, thus,

$$S(t) = e^{j\phi_{\vec{T}}(t)} \int f(\vec{u}) e^{-j\vec{\phi}_{\mathbf{R}}(t)\cdot\vec{u}} d\vec{u} \quad (8)$$

Hence, the signal collected at time t is the Fourier coefficient of our image at frequency location $\vec{\phi}_{\mathbf{R}}(t)$, multiplied by the phase adjustment term $\exp(j\phi_{\vec{T}}(t))$.

C. Motion Correction

If we know the motion of the patient with perfect accuracy and zero delay, we can, in principle, accommodate any patient motion by rotating the encoding gradients to follow the patient, and adjusting the phase of the resulting samples. If we use the inverse of the patient motion, then $\vec{\Phi}_{\mathbf{R}}(t)$ – our corrected version of $\vec{\phi}_{\mathbf{R}}(t)$ – becomes equal to $\vec{k}(t)$,

$$\vec{\Phi}_{\mathbf{R}}(t) = \gamma \int^t \mathbf{R}(\tau)\,\mathbf{R}^{-1}(\tau)\,\vec{G}(\tau)\,d\tau = \vec{k}(t)\,, \quad (9)$$

and $\Phi_{\vec{T}}(t)$ – our corrected version of $\phi_{\vec{T}}(t)$ – becomes

$$\phi_{\vec{T}}(t) = \gamma \int^t \mathbf{R}(\tau)\,\mathbf{R}^{-1}(\tau)\,\vec{G}(\tau)\cdot\left(-\vec{T}(\tau)\right)d\tau. \quad (10)$$

Hence, by rotating the gradient in real time and applying the phase correction term $\exp(-j\Phi_{\vec{T}}[n])$ to each sample, the measured signal becomes free of motion corruption, and is simply the Fourier transform of the image,

$$S\left(\vec{k}(t)\right) = F\left(\vec{k}(t)\right). \quad (11)$$

If the motion estimates are not perfect, then the rotations and translations we apply will not entirely reverse the effect of the motion. Suppose that $\mathbf{R}_a(t)$ and $\vec{T}_a(t)$ are approximations to $\mathbf{R}(t)$ and $\vec{T}(t)$, respectively. Using those motion estimates yields,

$$\vec{\Phi}_{\mathbf{R}}(t) = \gamma \int^t \mathbf{R}(\tau)\,\mathbf{R}_a^{-1}(\tau)\,\vec{G}(\tau)\,d\tau, \quad (12)$$

and

$$\Phi_{\vec{T}}(t) = \gamma \int^t \mathbf{R}(\tau)\,\mathbf{R}_a^{-1}(\tau)\,\vec{G}(\tau)\cdot\left(-\vec{T}_a(\tau)\right)d\tau. \quad (13)$$

This imperfect motion correction will still contain motion artifacts, but the closer $\mathbf{R}_a(t)$ and $\vec{T}_a(t)$ are to $\mathbf{R}(t)$ and $\vec{T}(t)$, the less artifact there will be.

III. Methods

A. MR Simulator

To demonstrate the effects of patient motion on image acquisition, and to test novel correction strategies using motion tracking data, an MR simulation program was developed based on a discrete-time version of the theory presented above.

Our MR simulator discretizes time, taking one step each 0.1 ms. That is, the strength of each scanner gradient is specified at 0.1 ms intervals. The patient motion is also specified for each time step. We represent discrete-time variables using an index with square brackets, such as $\vec{\phi}_{\mathbf{R}}[n]$ instead of $\vec{\phi}_{\mathbf{R}}(t)$. Hence, a time-discretized version of the phase integral in (7) is

$$\begin{aligned} \phi[n] &= \gamma\Delta t\left[\sum_{i=0}^{n-1}\mathbf{R}[i]\,\vec{G}[i]\right]\cdot\vec{u} - \gamma\Delta t\left[\sum_{i=0}^{n-1}\mathbf{R}[i]\,\vec{G}[i]\cdot\vec{T}[i]\right] \\ &= \vec{\phi}_{\mathbf{R}}[n]\cdot\vec{u} - \phi_{\vec{T}}[n]\,. \end{aligned} \quad (14)$$

Then we can rewrite our signal from (8) as

$$S[n] = e^{j\phi_{\vec{T}}[n]} \int f(\vec{u}) e^{-j\vec{\phi}_{\mathbf{R}}[n]\cdot\vec{u}} d\vec{u} \quad (15)$$

Hence, the signal collected at index n (i.e. at time $n\Delta t$) is the Fourier coefficient of our image at frequency location $\vec{\phi}_{\mathbf{R}}[n]$, multiplied by $\exp(j\phi_{\vec{T}}[n])$. We compute it using the FT of the test image, F, with

$$S\left(\vec{k}[n]\right) = e^{j\phi_{\vec{T}}[n]} F\left(\vec{\phi}_{\mathbf{R}}[n]\right). \quad (16)$$

We generate a motion-corrupted scan by sampling the FT of the test image, F, at $\vec{\phi}_{\mathbf{R}}[n]$ using nearest-neighbour interpolation, and then adjusting the phase.

Using this tracking data and the simulated MR data, we performed reconstructions using different methods: uncorrected, prospectively corrected using motion-tracking data, retrospectively corrected using motion-tracking data, and prospectively corrected using navigator echoes.

B. Tracking

Most motion-tracking systems cannot generate data at a rate of one sample every 0.1 ms. Rather, typical off-the-shelf systems generate data at a frequency of 30 Hz to 100 Hz. To simulate these systems, we down-sample our true motion information so that we attain a lower-frequency approximation of the motion-tracking data, which we will denote $\mathbf{R}_a[n]$ and $\vec{T}_a[n]$.

C. Uncorrected Reconstruction

The uncorrected reconstructions simply take the raw MR data (see (16)) and stores it in an array called $\tilde{F}(\vec{k})$. This array is a corrupted version of the ideal $F(\vec{k})$. The uncorrected reconstruction method generates an image by performing an inverse FFT on $\tilde{F}(\vec{k})$.

D. Prospective Reconstruction

In prospective reconstruction, the scan gradients are updated so that the scan plane follows the patient as they move. This method is implemented by counter-rotating the magnetic field gradients, giving us the approximately corrected phase state

$$\vec{\Phi}_{\mathbf{R}}[n] = \gamma \Delta t \left[\sum_{i=0}^{n-1} \mathbf{R}[i]\, \mathbf{R}_a^{-1}[i]\, \vec{G}[i] \right] \approx \vec{k}[n]\,. \qquad (17)$$

The translation can also be corrected by adjusting the phase,

$$\Phi_{\vec{T}} = \gamma \Delta t \left[\sum_{i=0}^{n-1} \mathbf{R}[i]\, \mathbf{R}_a^{-1}[i]\, \vec{G}[i] \cdot \left(-\vec{T}_a[i] \right) \right] \qquad (18)$$

Hence, our signal is

$$S\left(\vec{k}[n]\right) = e^{j\left(\Phi_{\vec{T}}[n] + \phi_{\vec{T}}[n]\right)} F\left(\vec{\Phi}_{\mathbf{R}}[n]\right), \qquad (19)$$

where $\Phi_{\vec{T}}[n] + \phi_{\vec{T}}[n]$ is close to zero for accurate motion-tracking.

E. Retrospective Reconstruction

While gradient control loops can be built into new scanners, it is a complicated and costly endeavour to add such a system to an existing machine. In such cases, the optical tracking device alone can be used in a retrospective correction scheme. Since we know the motion that occurred, we can apply the inverse of the motion to correct each and every sample in our corrupted data, $\tilde{F}$. As before, we compute the location of where the sample *should* have been placed using

$$\vec{\Phi}_{\mathbf{R}}[n] = \gamma \Delta t \left[\sum_{i=0}^{n-1} \mathbf{R}_a^{-1}[i]\, \vec{G}_{\mathbf{R}}[i] \right], \qquad (20)$$

where we use $\vec{G}_{\mathbf{R}}[i]$ to denote the (effectively) rotated gradients resulting from patient motion. Also, we apply a phase correction term based on the known translation, to get the retrospectively corrected data

$$S\left(\vec{\Phi}_{\mathbf{R}}[n]\right) = e^{j\Phi_{\vec{T}}[n]} \tilde{F}\left(\vec{\Phi}_{\mathbf{R}}[n]\right). \qquad (21)$$

Note that while the prospective technique dynamically corrects the scan trajectory to ensure all spatial frequencies are sampled as planned, the retrospective technique merely assigns the incorrectly acquired Fourier coefficients to the point in k-space they were actually sampled from. Spatial frequencies not sampled due to rotations of the scan trajectory cannot be retrieved. The retrospectively corrected reconstructions use the subsampled motion-tracking data ($\mathbf{R}_a[n]$ and $\vec{T}_a[n]$) to apply corrections to the k-space data according to (21).

F. Navigator Reconstruction

The navigator (NAV) corrected reconstructions use the motion-tracking data to prospectively update the scanning parameters once before each phase encoding. Recall that (17) and (18) show the effect of prospective scan correction. However, once the scan parameters are set, no more motion correction is done until the next phase encode. That is, any patient motion that occurs after the correction, but before the acquisition, manifests as motion corruption.

G. Experiments

To compare the effectiveness of the correction methods, we performed a small series of tests. In each test, a simulated stream of MR data was generated using a pulsed-gradient spin echo (PGSE) sequence (TR = 500 ms, TE = 100 ms). The MR samples were motion-corrupted using (16). The motion profile was a pseudo-periodic rotation about the z-axis with a period around 3 Hz and amplitude of approximately 1°.

We were also interested in how the refresh rate of the motion-tracking data would impact the motion-corrected reconstructions. Motion-tracking data was simulated at 30 Hz, 60 Hz, and 120 Hz by creating a piecewise constant motion function using a set-and-hold model.

Prospectively corrected reconstruction uses the sub-sampled motion-tracking data to update the scan parameters in real time, as in (17) and (18). Note, however, that since the motion is sub-sampled, the term $\mathbf{R}[i]\, \mathbf{R}_a^{-1}[i]$ will be slightly different than the identity operator, since the $\mathbf{R}_a^{-1}[i]$ lags somewhat behind the true rotation, $\mathbf{R}[i]$. The same is true for the phase correction term, since the translational motion-tracking data will be slightly different than the true translation. The four different methods were used to reconstruct the data.

To compare the four reconstruction methods, we compute the sum of squared differences (SSD) between the original image and the reconstructed image.

IV. Results

Table I shows the SSD for the various reconstruction methods at different motion-tracking data rates. The uncorrected images yield an SSD of 1759 (independent of motion-tracking data rate). Not surprisingly, the retrospective and prospective reconstructions get better (lower SSD) as the motion-tracking data rate increases from 30 Hz to 120 Hz. The navigator method is also independent of the motion-tracking frequency because the method does not depend on a motion-tracking system, but rather determines motion from information collected by the scanner itself.

TABLE I
SSD OF RECONSTRUCTIONS

Motion-Tracking freq.	Uncorr.	NAV	Retro.	Prosp.
30 Hz	1759	1023	1228	1019
60 Hz	1759	1023	1234	360
120 Hz	1759	1023	922	138

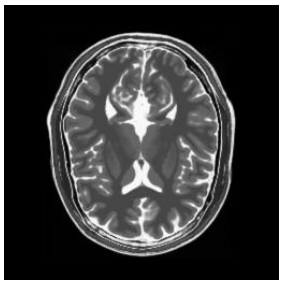

(a) Original

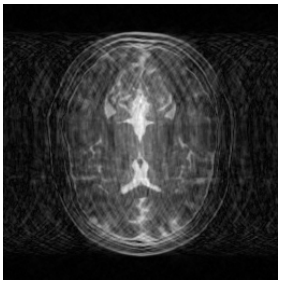

(b) Uncorrected

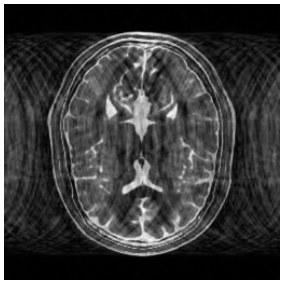

(c) Navigator

Fig. 1. BrainWeb test image, and two reconstructions

Figure 1(a) shows the original BrainWeb T1-weighted image that was used for testing, while (b) shows the uncorrected reconstruction, and (c) shows the navigator reconstruction. As the update frequency of the motion-tracking data increases, the reconstructions that use that data (retrospective and prospective methods) get more and more accurate. The navigator method performs about as well as the retrospective method at 120 Hz, and the prospective method at 30 Hz. However, the prospective method outperforms the other methods as the motion-tracking data rate increases.

Figures 2-4 show the retrospective and prospective reconstructions that use the motion-tracking data at 30 Hz, 60 Hz, and 120 Hz, respectively. Clearly, as the frequency of the motion-tracking data increases, the motion artifacts in the reconstructions visibly diminish. Moreover, the prospective method contains substantially less artifact, consistent with the SSD results shown in Table I.

V. CONCLUSIONS

Generally speaking, the more frequently motion information was incorporated into the reconstruction method, the better the images were. In particular, both the retrospective and prospective methods improved as the motion-tracking sample frequency increased. However, the fact that the navigator echo method performs about as well as the retrospective method at 120 Hz suggests that much is gained when the motion is corrected by adjusting the scan parameters, rather than trying to undo the motion as a post-processing step. Updating the scan plane just *once* for each phase encode was as good as using 120 Hz motion-tracking data to perform retrospective correction.

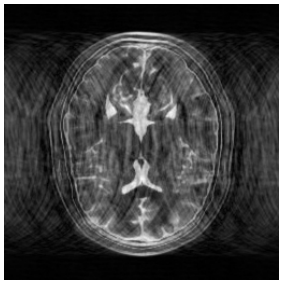

(a) Retrospective

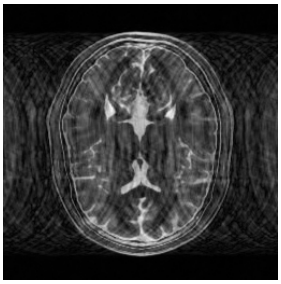

(b) Prospective

Fig. 2. BrainWeb reconstructions using 30 Hz motion-tracking data

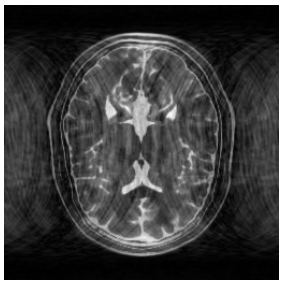

(a) Retrospective

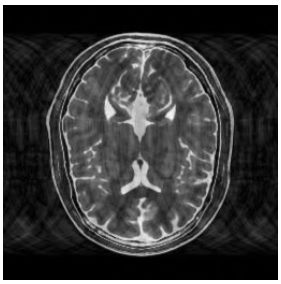

(b) Prospective

Fig. 3. BrainWeb reconstructions using 60 Hz motion-tracking data

Future work includes testing the robustness of these reconstruction methods when the motion-tracking data has errors and time delays. Since this study is a simulation, further validation on a real system is necessary.

ACKNOWLEDGMENT

The authors thank the Montreal Neurological Institute for the use of their BrainWeb data. The authors are also thankful to the Natural Science and Engineering Research Council of Canada and the Canada Foundation for Innovation for funding of this project.

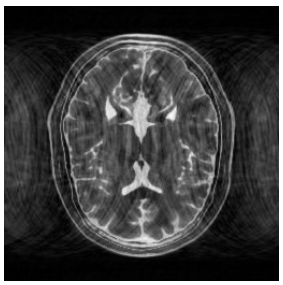

(a) Retrospective

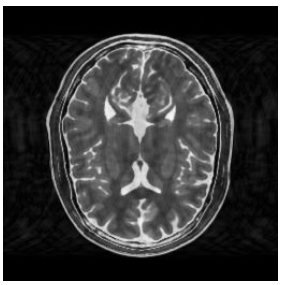

(b) Prospective

Fig. 4. BrainWeb reconstructions using 120 Hz motion-tracking data

REFERENCES

[1] D. Atkinson and D. L. G. Hill, "Automatic correction of motion artifacts in magnetic resonance images using an entropy focus criterion," *IEEE Trans Med Imaging*, vol. 16, no. 6, pp. 903–910, 1997.

[2] R. L. Ehman and J. P. Felmlee, "Adaptive technique for high-definition MR imaging of moving structures," *Radiology*, vol. 173, no. 1, pp. 255–263, 1989.

[3] M. Tremblay, F. Tam, and S. J. Graham, "Retrospective coregistration of functional magnetic resonance imaging data using external monitoring," *Magn Reson Med*, vol. 51, no. 1, pp. 141–149, 2005.

[4] M. Zaitsev, C. Dold, G. Sakas, J. Henning, and O. Speck, "Magnetic resonance imaging of freely moving objects: Prospective real-time motion correction using an external optical motion tracking system," *NeuroImage*, vol. 31, pp. 1038–1050, July 2006.

[5] R. J. Ordidge, J. A. Helpern, Z. X. Qing, R. A. Knight, and V. Nagesh, "Correction of motional artifacts in diffusion-weighted mr images using navigator echoes," *MRI*, vol. 12, no. 3, pp. 455–460, 1994.

[6] A. W. Anderson and J. C. Gore, "Analysis and correction of motion artifacts in diffusion weighted imaging," *Magn Reson Med*, vol. 32, pp. 379–387, 1994.

[7] T. P. Trouard, Y. Sabharwal, M. I. Altbach, and A. F. Gmitro, "Analysis and comparison of motion-correction techniques in diffusion-weighted imaging," *J Magn Reson Imaging*, vol. 6, pp. 925–935, 1996.

[8] R. A. Zoroofi, K. Homma, Y. Sato, S. Tamura, and H. Naito, "Technique for reduction of MRI 3-D affine motion artifacts," in *Proceedings of SPIE Medical Imaging*, San Diego, 2000, pp. 1625–1634.

[9] C. Dold, M. Zaitsev, O. Speck, E. A. Firle, J. Henning, and G. Sakas, "Prospective head motion compensation for MRI by updating the gradients and radio frequency during data acquisition," in *Medical Image Computing and Computer-Assisted Intervention (MICCAI'05)*, vol. 8, no. 1, 2005, pp. 482–489.

[10] C. Dold, M. Zaitsev, O. Speck, E. A. Firle, and J. H. amd Georgios Sakas, "Advantages and limitations of prospective head motion compensation for MRI using an optical motion tracking device," *Academic Radiology*, vol. 13, no. 9, pp. 1093–1103, September 2006.

[11] Z.-P. Liang and P. C. Lauterbur, *Principles of Magnetic Resonance Imaging: A Signal Processing Perspective*. Bellingham, Washington: SPIE Press, 2000.